

Testing the modified HIRLAM radiation scheme

Laura Rontu and Simo Järvenoja (FMI)

Several modifications to the HIRLAM radiation scheme (Savijärvi, 1990; Sass et al., 1994; Wyser et al., 1999) have been implemented and tested. In addition to the standard verification, diagnostic tools available in the reference HIRLAM system have been used in the comparisons. Here, we describe shortly the modifications and the experimental setup. Use of the diagnostic variables is discussed and results of the model comparisons are shown.

1 Modifications

Clear sky short-wave radiation

Modifications proposed by Räisänen et al. (2000) were implemented: absorption of ozone is taken into account when calculating the atmospheric heating due to short-wave radiation and a small correction of the SW albedo zenith angle dependency is made.

Cloudy sky short-wave radiation

Two minor coding errors affecting the arrival at the cloud top and absorption in cloud of the down-welling short-wave radiation were corrected. Cloud heterogeneity effects were included in a crude way by decreasing the cloud cover by 20 % before the calculation of cloud SW absorption and reflection.

Clear sky long-wave radiation

Modifications proposed by Räisänen et al. (2000) were implemented: Water vapour emissivity was replaced by total gaseous emissivity, including also the carbon dioxide. Water vapour continuum absorption is treated in a consistent way instead of the previous empirical formulation. The modifications also included a few smaller technical corrections.

Cloudy sky long-wave radiation

A modification of the LW flux below clouds (Colin Jones, personal communication) was implemented. The clear sky contribution to LW flux at the surface is now a combination of the clear sky flux from the whole depth of atmosphere in the clear portion of the grid box, plus a clear sky contribution from below the cloud base.

Surface short-wave albedo

The value of snow albedo over low vegetation surface was adjusted from 0.51 to 0.36.

Surface long-wave emissivity

Different emissivity values for different surface types based on Wilber et al. (1999) were introduced as follows:

water	0.97
ice	0.99
bare land	0.90
low vegetation	0.97
forest	0.98
snow	0.98

Compared to the previous constant value of 0.95 the emissivity is thus increased for most surface types.

Use of surface emissivity when calculating atmospheric long-wave heating

In the previous formulation surface emissivity was taken into account only when calculating the surface energy balance but not when handling the atmospheric LW heating. Now the surface emissivity is included also here. The small contribution of reflected from the surface LW radiation is added into the up-welling flux.

Radiation - ISBA - diagnostics interface

In the HIRLAM code, the task of the radiation parametrization (RADIA) is to calculate the atmospheric radiative heating and the down-welling and up-welling radiative fluxes at the surface and at the top of the atmosphere (TOA). For these calculations averaged over the grid square values of surface emissivity, albedo and skin temperature are needed. The surface parametrization scheme (ISBA) handles the surface energy balance. The balance is calculated separately over bare and snow-covered surface subtypes. Here, corresponding net radiative fluxes over every subtype are needed. The code was reorganized to handle these processes consistently and also produce the correct diagnostic output.

2 Experiments

To see the effect of the modifications, a parallel experiment similar to the northern spring test case of ISBA (Rodriguez et al., 2003) was run on the Finnish IBM eServer Cluster 1600 system.

The reference experiment RE6 used the HIRLAM 6.0.0 code. The experiment RMP included all the radiation modifications and, passively, code related to mesoscale orography parametrizations (Rontu et al., 2002) and enhanced postprocessing (Rontu and Fortelius, 2000). Both experiments included their own data assimilation cycles.

Properties common to the experiments were:

- domain 186 x 138, resolution 0.2 deg, 31 levels, Northern European area
- Semi-Lagrangian dynamics with a time step of 300 s
- 3DVAR analyses with a 6h assimilation cycle

- lateral boundaries based on analyses¹
- +48h forecasts from 00UTC analyses only
- period 12-26 April 1998

3 Diagnostics

The available accumulated variables in the HIRLAM reference system are documented in Undén et al. (2002) (Appendix)². They include heat and moisture fluxes at the surface and TOA and three-dimensional and integrated over the depth of the atmosphere heat and moisture tendencies due to the different parametrizations. (Corresponding momentum fluxes and tendencies are also available in the modified code of RMP.) For the present model comparison, three-dimensional temperature tendencies plus radiative fluxes at the surface and TOA were used.

The change of temperature is given by

$$\frac{\partial T(x, y, z, t)}{\partial t} = \frac{\partial T}{\partial t}_{dyn} + \frac{\partial T}{\partial t}_{phys} = \vec{v} \cdot \nabla T + \frac{\alpha\omega}{c_p} + \frac{1}{c_p}[Q_{rad} + Q_{cond} + Q_{turb}], \quad (1)$$

$$\begin{aligned} Q_{rad} &= -\frac{1}{\rho} \frac{\partial F_{rad}}{\partial z} \\ \text{where } Q_{cond} &\approx L(E_c - C_c + E_p) \\ Q_{turb} &= -\frac{1}{\rho} \frac{\partial c_p \rho \theta' w'}{\partial z} \end{aligned}$$

and E_c , C_c and E_p denote evaporation and condensation of cloud condensate and evaporation of precipitation and c_p specific heat of dry air. The term $\alpha\omega$ represents conversion between kinetic energy and enthalpy.

Integrating vertically we obtain

$$\widehat{\frac{\partial T}{\partial t}}_{phys} = \int_0^{p_s} \frac{\partial T}{\partial t}_{phys} \frac{dp}{g} = \frac{1}{c_p}[\widehat{Q}_{rad} + \widehat{Q}_{cond} + \widehat{Q}_{turb}], \quad (2)$$

where the integrated source terms reduce to their corresponding boundary values

$$\widehat{Q}_{rad} = -(F_{rad})_{TOA} + (F_{rad})_{SFC} \quad (3)$$

$$\widehat{Q}_{turb} = H \quad (4)$$

$$\widehat{Q}_{cond} \approx L(P_R + \frac{\partial c}{\partial t}_{phys}) + L_i P_S, \quad (5)$$

where F_{rad} is the radiative flux intensity at surface (SFC) and at the top of the atmosphere (TOA), H is the sensible heat flux, L and L_i are the latent heat of condensation and fusion,

¹The first cycle of experiments used ECMWF analyses. In the second cycle, where a few technical corrections were made to the code, the analyses of the previous cycle of the same experiment were used as boundaries without interpolations.

²In the printed version, units of some of the accumulated variables are incorrect. See the updated version in HexNet for corrections.

correspondingly, P_R and P_S denote rain and snow precipitation and c is the cloud condensate. Thus, the vertically integrated heating due to the physical parametrizations is determined by the surface and the TOA fluxes.

Technically, requesting the needed diagnostic output of a HIRLAM experiment is simple. The needed variables are included into a postprocessing list, e.g. of the md file defined in the script FCinput. A redefinition of the parameters defining the array dimensions may be needed (in namelist &namprc given in FCinput: `iacdg2=16,iacdg=8,`) The results can be handled by any visualization software capable of reading GRIB files.

4 Results

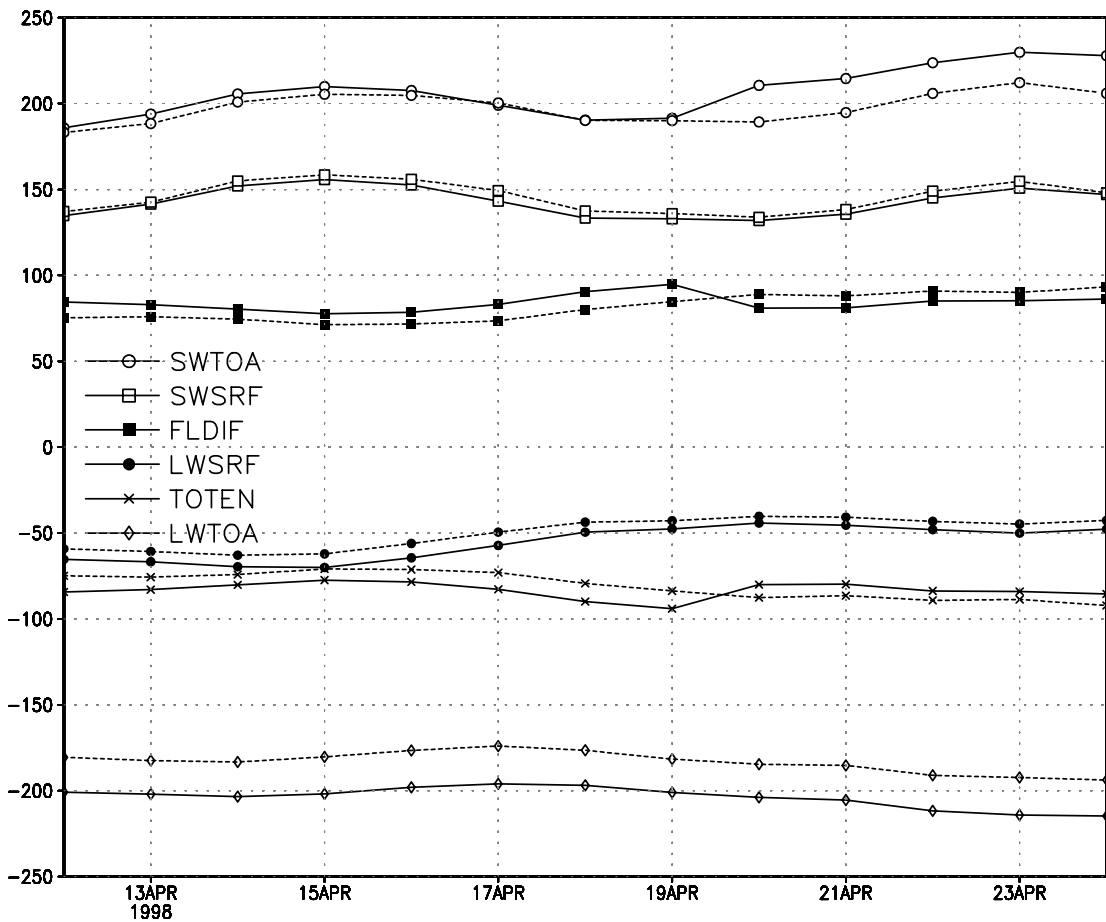


Figure 1: Area-averaged net radiative fluxes and heating of the atmosphere [Wm^{-2}], based on +48h forecasts. Solid lines: results of experiment RMP, dashed lines: results of the reference run RE6. Short-wave flux at TOA - open circles, short-wave flux at surface - open squares, difference of TOA and surface net fluxes - filled squares, long-wave flux at surface - filled circles, vertically integrated temperature tendency due to radiation - crosses, long-wave flux at TOA - open diamonds. Downward fluxes are denoted positive.

Fig. 1 shows the time series of vertically integrated temperature tendency due to the radiation parametrizations and of the radiative fluxes averaged over the whole integration area, for both experiments (+48h forecasts), i.e. all components of the following equation

$$c_p \overline{\frac{\partial T}{\partial t}}_{rad} = -\overline{(F_{SW})_{TOA}} + \overline{(F_{SW})_{SFC}} - \overline{(F_{LW})_{TOA}} + \overline{(F_{LW})_{SFC}},$$

where the overline denotes an area average.

First, we see that the total heating indeed corresponds to the flux difference for both of the experiments. This elementary check confirms that the boundary conditions and heating are correctly formulated in the code. Second, the integrated radiative cooling of the atmosphere is stronger in the modified experiment RMP during the first week of the experiment and weaker during the last days, when the net short-wave flux at the top of the atmosphere increases in RMP. This seems to be due to the corrections in cloud short-wave absorption, as the difference largely comes from areas with mostly clear sky in the beginning and cloudy in the end of the comparison (not shown). The up-welling long-wave radiative flux at the top of the atmosphere is larger all the time. When looking at the averaged map of the difference between the predicted TOA LW fluxes (not shown), one can see that in RMP this flux is larger than in RE6 everywhere over the integration area. This might be connected with the increased surface emissivity. Comparison with the satellite measurements would be needed to understand if the increase is realistic. Differences between the experiments of all surface fluxes and SW TOA flux are smaller.

Fig. 2 depicts the vertical distribution of the temperature tendencies, averaged in time and over the area, due to the different parametrizations as given by the +48h forecasts of both experiments, i.e. the Q-terms of the following equation:

$$\overline{\frac{\partial T(z)}{\partial t}}_{phys} = \frac{1}{c_p} (\overline{Q_{rad}} + \overline{Q_{cond}} + \overline{Q_{turb}})$$

Note that the tendency at every model layer, independently of the layer thickness, is shown with equal weight. In both experiments radiation tends to cool the whole troposphere. Cooling rate given by RMP is smaller than that of RE6 in upper troposphere and in the stratosphere. It is larger in the middle and lower troposphere, especially at the lowest model level. The differences at upper levels are most probably connected with corrections in the short-wave absorption by ozone and clouds. The lowest layer differences could be due to the changes related to surface long-wave emissivity (and short-wave albedo). In both experiments the turbulence tends to balance the cooling due to radiation in the lowest troposphere. Heating due to condensation is quite similar in the experiments.

Based on these results, one could expect that the modifications might lead to slightly less near-surface temperatures and possibly to slightly higher upper layer temperatures. The systematic difference RMP-RE6 of the two-metre temperatures (Fig. 3) indeed shows that in Central Eastern Europe the temperature is somewhat colder while in the North, daytime temperatures have locally even increased. Close to the pressure level 850 hPa the temperatures are slightly colder, close to the level 300 hPa slightly warmer (maps not shown) in RMP than in RE6.

The results of station verification of the surface pressure and screen level temperature are shown in Fig. 4. One can see slight improvement in both parameters. The scores related to wind and humidity did not show any significant difference nor did the values of any parameters at upper levels.

199804(12-24)00+48

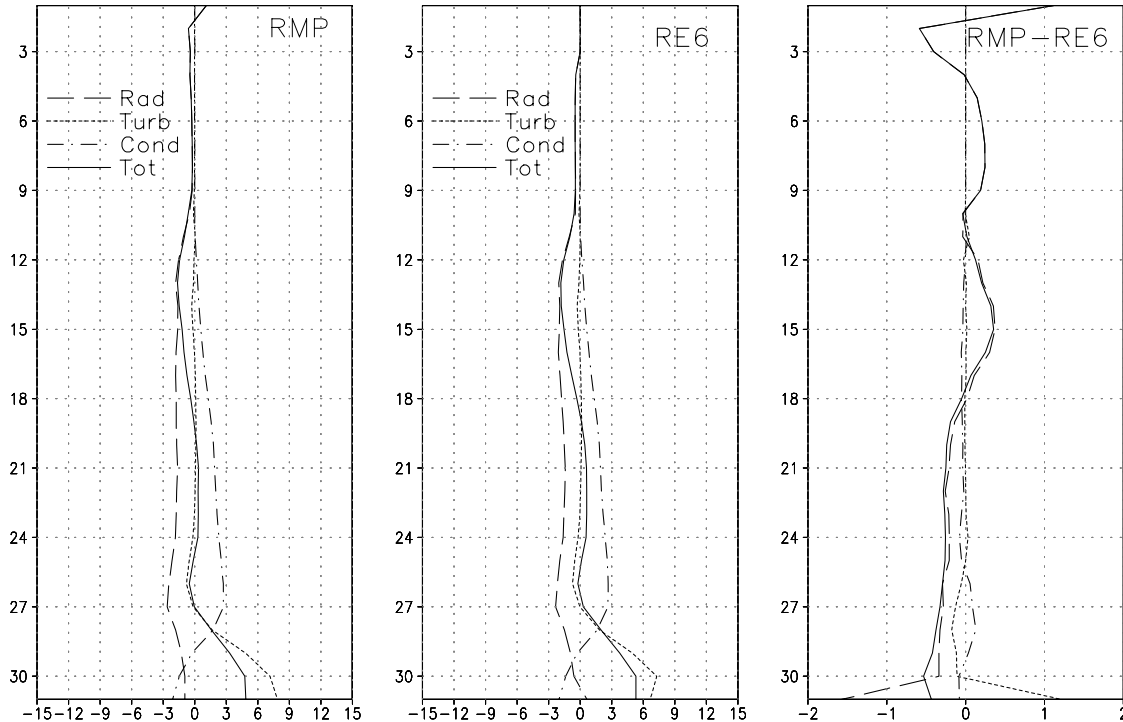


Figure 2: Vertical distribution of area-averaged temperature change during the +48h forecasts $[K/48h]$ due to the different parametrizations for experiments RMP (left) and RE6 (middle) and their difference (right). Solid lines: total tendency, dashed: contribution of radiation, dotted: turbulence, dash-dotted: condensation. Levels in vertical between surface and the level of 10 hPa are shown on the y-axis.

5 Conclusions

Modifications to the HIRLAM radiation code were tested during one two-week spring-time parallel run. Diagnostics and verification showed that the modified scheme tends to cool the lower atmosphere more and the upper atmosphere less than the reference scheme. Slight improvement in the verification scores was detected. The behaviour of the modified code was stable. It required no more computing time than the present scheme. It is proposed to implement the changes into the reference system after a few additional tests, which would include single-column comparisons with the ICRCCM data and parallel runs for winter (January 2000) and summer (June 1997) periods.

Acknowledgements

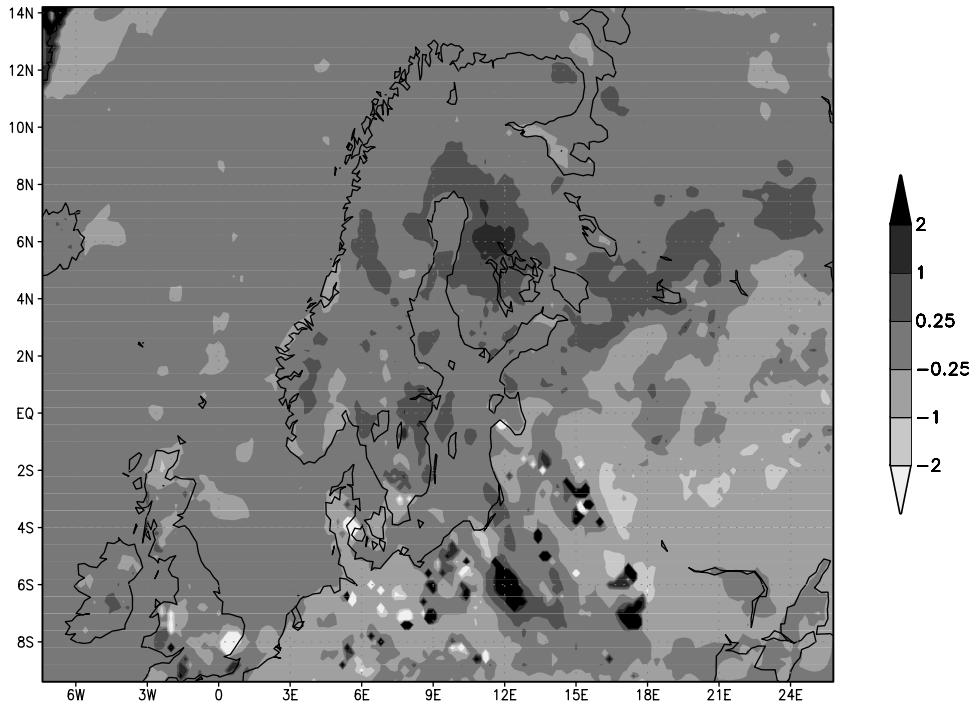
Several persons have recently contributed to the improvement of the radiation code: Petri Räisänen wrote the code of modifications proposed in Räisänen et al. (2000). Colin Jones wrote the code for the long-wave-below-clouds modification and proposed the modification of handling surface long-wave emissivities in the atmospheric calculations. Markku Rummukainen and Anastasya Senkova found several coding errors in the earlier versions of RADIA. Carl

Fortelius participated in the formulation of the diagnostic output from radiation. The comments of Ernesto Rodriguez and Stefan Gollvik helped in formulation of the ISBA-radiation interface.

References

- Rodriguez, E., B. Navascues, J.J. Ayuso and S. Järvenoja, 2003. Analysis of surface variables and parameterization of surface processes in HIRLAM. Part I: Approach and verification by parallel runs. HIRLAM Technical Report, 58, 52 pp. Norrköping, January 2003. Available at <http://www.knmi.nl/hirlam>.
- Rontu L., K.Sattler, and R. Sigg, 2002. Parametrization of subgrid-scale orography effects in HIRLAM. HIRLAM Technical Report 56, 46 pp. Norrköping, October 2002. Available at <http://www.knmi.nl/hirlam>.
- Rontu, L. and C. Fortelius, 2000. Recent developments in postprocessing. HIRLAM Newsletter, 36, 80-88. Available at <http://www.knmi.nl/hirlam>.
- Räisänen, P. , M. Rummukainen and J. Räisänen, 2000. Modification of the HIRLAM radiation scheme for use in the Rossby Centre regional atmospheric climate model. Department of Meteorology, University of Helsinki. Technical report 49, 71 pp. Available at <http://www.meteo.helsinki.fi/Reports.html>.
- Sass, B. H. and L. Rontu and P. Räisänen, 1994. HIRLAM-2 Radiation Scheme: Documentation and Tests. HIRLAM Technical Report, 16, 43 pp. Norrköping, November 1994. Available at <http://www.knmi.nl/hirlam>.
- Savijärvi, H, 1990. Fast radiation parameterization schemes for mesoscale and short-range forecast models. J. Appl. Meteor., 29, 437-447.
- Undén, P. and coauthors, 2002. HIRLAM-5 Scientific Documentation. 144 pp. Norrköping. Available at <http://www.knmi.nl/hirlam>.
- Wilber A. A., D. P. Kratz and S. K. Gupta, 1999. Surface Emissivity Maps for Use in Satellite Retrievals of Longwave Radiation. TP- 1999-209362, August 1999, pp. 35. Available at <http://techreports.larc.nasa.gov/ltrs/PDF/1999/tp/NASA-99-tp209362.pdf>
- Wyser, K. and L. Rontu and H. Savijärvi, 1999. Introducing the effective radius into a fast radiation scheme of a mesoscale model. Contrib. Atm. Phys., 72, 205-218.

Systematic difference of two-metre temperature (K)
199804(12-24)00+36 RMP-RE6



Systematic difference of two-metre temperature (K)
199804(12-24)00+48 RMP-RE6

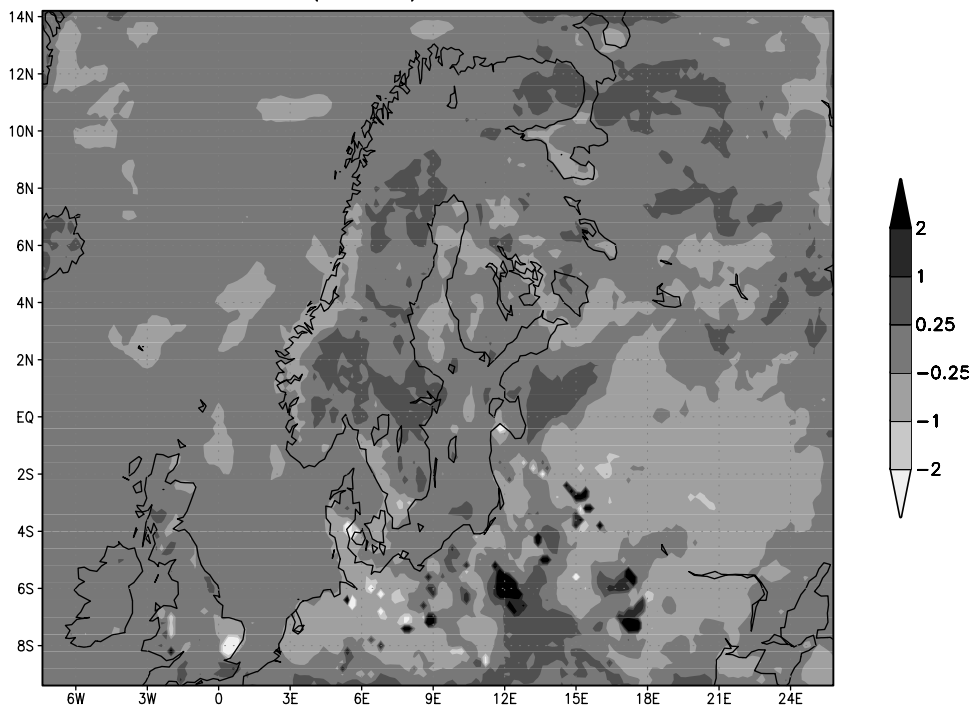


Figure 3: Systematic difference of the screen level temperatures [K] RMP-RE6. Forecasts valid at daytime (+36h): upper panel and at nighttime (+48h): lower panel.

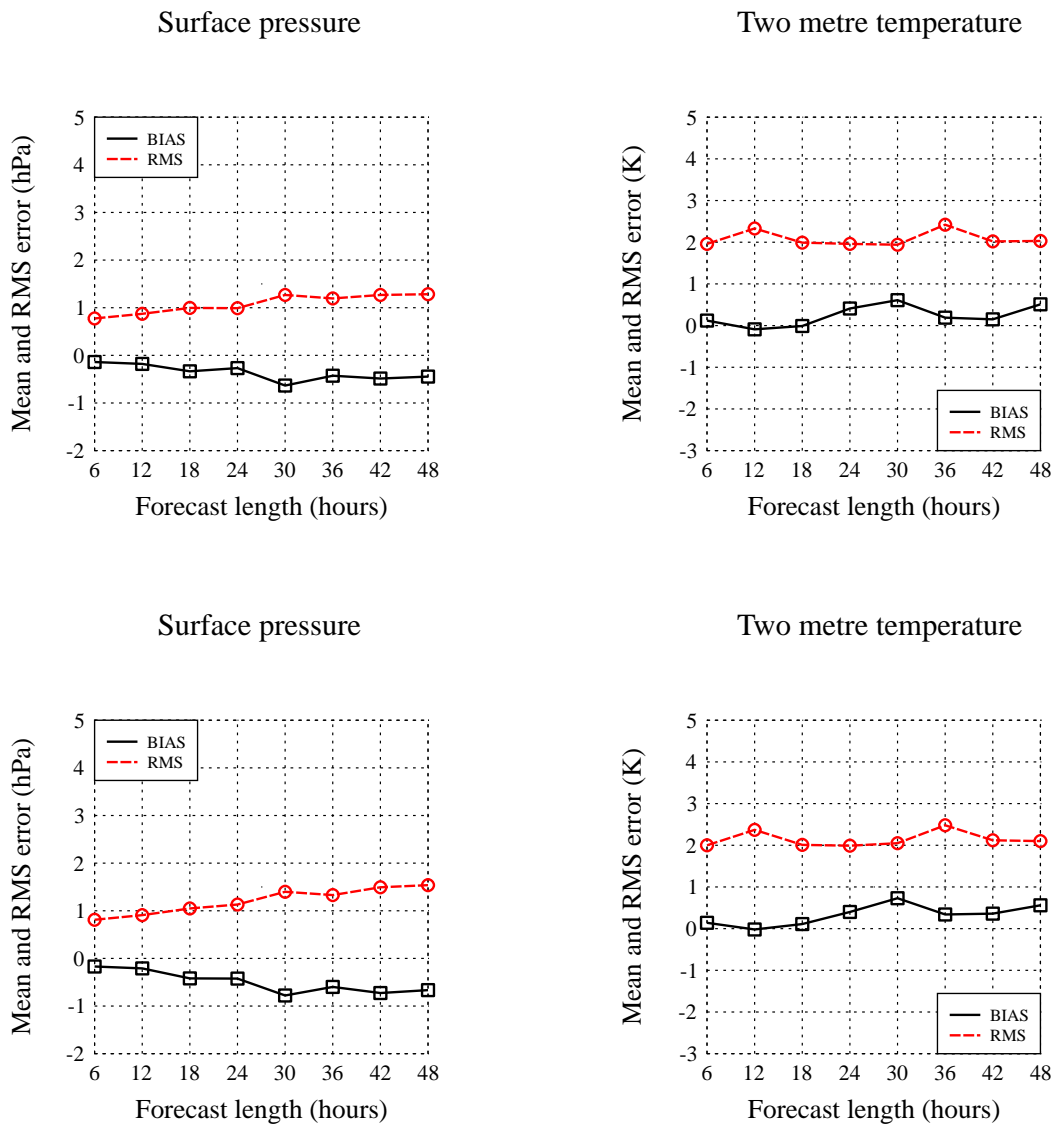


Figure 4: Results of station verification as a function of forecast length over EWGLAM stations for surface pressure (left) and screen level temperature (right), experiments RMP (upper figures) and RE6 (lower figures), for the forecasts starting at 00 UTC only.